Nickel and GTP Modulate Helicobacter pylori UreG Structural Flexibility

Annalisa Pierro, Emilien Etienne, Guillaume Gerbaud, Bruno Guigliarelli, Stefano Ciurli, Valérie Belle, Barbara Zambelli, Elisabetta Mileo

Nickel and GTP modulate *Helicobacter pylori* UreG structural flexibility.

Annalisa Pierro,[1] Emilien Etienne,[1] Guillaume Gerbaud,[1] Bruno Guigliarelli,[1] Stefano Ciurli,[2] Valérie Belle,[1] Barbara Zambelli,[2,* Elisabetta Mileo.[1,*]

[1] Aix Marseille Univ, CNRS, BIP, Bioénergétique et Ingénierie des Protéines, IMM, Marseille, France.
[2] University of Bologna, Laboratory of Bioinorganic Chemistry, Department of Pharmacy and Biotechnology, Bologna, Italy.
* Correspondence: Corresponding author.

Abstract: UreG is a P-loop GTP hydrolase involved in the maturation of nickel-containing urease, an essential enzyme found in plants, fungi, bacteria and archaea. This protein couples the hydrolysis of GTP to the delivery of Ni(II) into the active site of apo-urease, interacting with other urease chaperones in a multi-protein complex necessary for enzyme activation. Whereas the conformation of *Helicobacter pylori* (*Hp*) UreG was solved by crystallography when it is in complex with other two chaperones, in solution the protein was found in a disordered and flexible form, defining it as an intrinsically disordered enzyme and indicating that the well-folded structure found in the crystal state does not fully reflect the behavior of the protein in solution. Here, isothermal titration calorimetry and Site-Directed Spin Labeling coupled to Electron Paramagnetic Spectroscopy were successfully combined to investigate *Hp*UreG structural dynamics in solution and the effect of Ni(II) and GTP on protein mobility. The results demonstrate that, although the protein maintains a flexible behaviour in the metal and nucleotide bound forms, concomitant addition of Ni(II) and GTP exerts a structural change through the crosstalk of different protein regions.

1. INTRODUCTION

The discovery of antimicrobials to defeat bacterial pathogens is among the most important medical advances of the last century. However, antimicrobial resistance (AMR) has impaired the efficacy of antibiotics against infections in the last decades, and is considered by the World Health Organization (WHO) as one of the most important threats to public health for the next future.[1-2] In 2017, WHO listed the twelve most important resistant bacteria at a global level for which there is urgent need for new therapies.[3] Ten of them produce the virulence factor urease, a nickel-enzyme that hydrolyzes urea to produce ammonia and carbamate, thus leading to pH increase.[4] This event provides a suitable environment for host colonization, both by producing a micro-environment compatible with bacterial growth and by supplying nitrogen sources. For example, *Staphylococcus aureus* urease activity determines biofilm formation and is required for bacterial persistence,[5-6] while for *Proteus mirabilis*,[7] *Staphylococcus saprophyticus*[8] and *Ureaplasma ureolyticum*[9] urease activity plays a central role for infection and urea stones formation in the urinary tract. Several of these pathogens are involved in bacterial infections of the respiratory apparatus. It is remarkable that half of patients who died of the recent CoViD19 epidemics in Wuhan (China) became co-infected with bacteria in the lungs and also required antibiotics.[10] Therefore, urease is an attractive target for the development of

44 innovative antibacterial molecules, acting both as antibiotics, as well as preventive anti-virulence
45 drugs or adjuvants for bacterial eradication.
46   One of the best-known pathogens that exploits the enzymatic activity of urease is the Gram-
47 negative bacterium *Helicobacter pylori*, a widespread microbe, infecting the stomach of up to 50% and
48 80% of adults in industrialized and developing countries, respectively.[11] The infection causes chronic
49 inflammation of the gastric mucosa, which can slowly progress to gastric ulcer and, through the
50 premalignant stages of atrophic gastritis, to gastric adenocarcinoma or gastric mucosa-associated
51 lymphoid tissue (MALT) lymphoma. In 1994 the WHO classified *H. pylori* as a class I carcinogen. The
52 neutralization of pH driven by urease is required by *H. pylori* for the colonization of the gastric niche,[12]
53 while the generated ammonia and induced platelet activation also plays a critical role in the
54 inflammatory response of the host and in the progress of the disease.[13]
55   Bacterial ureases are generally heteropolymeric proteins with a quaternary structure $(\alpha\beta\gamma)_3$.[4, 14-
56 15] In the genus *Helicobacter*, the trimer is of the type $(\alpha\beta)_3$, with the β subunits corresponding to the
57 fused β and γ subunits normally found in other bacteria. The protein also presents a higher level of
58 oligomerization with a $[(\alpha\beta)_3]_4$ quaternary structure.[16] Despite the different oligomeric organization,
59 the structure of the known urease enzymes is fully conserved, and they present a substantially
60 identical active site found in the α subunit. This site contains two Ni(II) ions bridged by the
61 carboxylate group of a carbamylated lysine, essential to maintain the ions at the correct distance for
62 catalysis, and by a hydroxide ion, the nucleophile in the hydrolysis reaction.[4, 14-15]
63   Although previous studies identified several molecules that bind urease and inhibit it
64 competitively or uncompetitively, none of them is generally used in therapy, due to their severe side
65 effects or limited ability to pass the bacterial membrane.[14-15] Recently, an alternative strategy to design
66 urease inhibitors has been proposed by targeting, instead of the enzyme, the process that delivers
67 nickel ions into the enzyme active site, precluding enzyme maturation to the active Ni(II)-loaded
68 urease.[17] This activation process is governed by the interplay of at least four accessory proteins,
69 named UreD, UreE, UreF and UreG, coded by genes belonging to a single operon together with the
70 structural genes.[4] UreE acts as the metallo-chaperone of the system that delivers Ni(II) into urease,[18]
71 through tunnels that pass across a complex formed by UreD, UreF and UreG, the last acting as a
72 molecular chaperone that prepares urease to incorporate the metal ion.[19] Precluding urease
73 maturation by blocking delivery of Ni(II) into its active site could thus represent a novel approach to
74 enzyme inhibition.
75   The central player of the urease chaperone activation network is UreG, a GTPase that couples
76 the energy obtained from GTP hydrolysis to urease maturation.[20] *Hp*UreG interacts either with
77 *Hp*UreE, forming a heterodimeric *Hp*UreG$_2$E$_2$ complex,[18] or with *Hp*UreF and *Hp*UreD, forming a
78 ternary *Hp*UreG$_2$F$_2$D$_2$ complex.[21] The multiplicity of partners of UreG is reflected in its folding
79 flexibility: while the structure of the protein has been reported for the GDP-bound *Hp*UreG in the
80 *Hp*UreG$_2$F$_2$D$_2$ complex,[21] and for the GMPPNP (guanylyl imidodiphosphate)-bound *Klebsiella*
81 *pneumonia* (Kp) UreG,[22] in solution, both *Hp*UreG and *Kp*UreG feature high flexibility in solution, as
82 shown by NMR spectroscopy, suggesting that the single conformation determined by X-ray
83 crystallography does not reflect the flexible behavior of the protein in solution. This behavior is more
84 generally observed in ^{1}H,^{15}N-HSQC NMR spectra of a plethora of UreG homologues from bacteria,
85 archaea and plants, which show broad signals with limited spread in the ^{1}H dimension, indicating a
86 backbone mobility in the intermediate exchange regime.[23-26] Native mass spectrometry and Site-
87 Directed Spin Labeling coupled to Electron Paramagnetic Resonance (SDSL-EPR) confirmed the
88 presence of a heterogeneous conformational landscape for *Sporosarcina pasteurii* (*Sp*) UreG in the gas
89 phase and in solution respectively, with at least two conformers with different degree of folding that
90 coexist in equilibrium.[27-28]
91   The selection of the binding partner is defined by the nucleotide bound state of the protein: GTP
92 binding facilitates the formation of the *Hp*UreG$_2$E$_2$,[29] while the GDP-bound form preferentially
93 interacts in the *Hp*UreG$_2$F$_2$D$_2$ complex.[30] In addition, the concomitant presence of Ni(II) and GTP
94 drives UreG dimerization in solution.[30] Ni(II) binds to a conserved Cys-Pro-His (CPH) motif, located
95 on the protein interaction surface,[31] while GTP binds on the opposite side of the protein.[29]

96   A comparison of the crystal structure of the GMPPNP-bound *Kp*UreG and the GDP-bound UreG
97 in the *Hp*UreG$_2$F$_2$D$_2$ complex suggested that the presence of GTP drives an allosteric modulation of
98 the Ni(II) binding site, which assumes a square planar geometry able to accommodate Ni(II),[22]
99 suggesting that the two protein regions that bind Ni(II) and GTP/GDP communicate by allostery to
100 drive the necessary conformational changes for UreG to function. However, such allosteric effect has
101 not been proven in solution. The present study addresses this point, combining multiple biophysical
102 approaches: SDSL- EPR, Isothermal Titration Calorimetry (ITC) and static and dynamic light
103 scattering (MALS-QELS).
104   In particular, we targeted three different regions of the protein with nitroxide-based spin labels
105 and we performed both continuous wave and pulsed EPR spectroscopy in the presence of Ni(II) and
106 GTP in order to determine their effect on the structural dynamics of *Hp*UreG in solution, as well as
107 to investigate the structural crosstalk of different protein regions occurring by flexibility modulation.
108 The results obtained were complemented by ITC and MALS-QELS. Altogether the results show that
109 the concomitant addition of both Ni(II) and GTP induces a modification of the structure and mobility
110 in two regions of the protein.
111

112 **2. RESULTS AND DISCUSSION**

113 *2.1. Cys variants were generated to selectively label distinct regions of HpUreG*

114   SDSL-EPR spectroscopy is a non-destructive technique that provides details on protein structure
115 and flexibility over a wide-range of temperatures and timescales.[32-35] Proteins can be studied in their
116 native environment, that is in membranes, in cellular extract and also inside cells.[36] SDSL-EPR
117 involves the grafting of a paramagnetic label, generally a thiol-specific nitroxide, on the protein of
118 interest and the determination of the dynamic properties of the attached nitroxide by continuous
119 wave (CW)-EPR spectroscopy.[37-38] Changes in the nitroxide spectrum are thoroughly related to the
120 mobility of the nitroxide side-chain and to the local backbone motion, which can thus be used to
121 follow protein structural changes and to reveal interaction sites in complexes in solution and at room
122 temperature. [37, 39-42] Distance distributions between two spin labels can be measured by pulsed Double
123 Electron-Electron Resonance (DEER) techniques relying on their dipole-dipole coupling.[43-44] Inter-
124 label distance ditributions can be investigated between 15 and 80 Å, but in specific experimental
125 conditions, 160 Å can be reached.[45] DEER experiments are usually carried out at cryogenic
126 temperature (60 K), the low temperature being required to slow down the otherwise fast relaxation
127 of nitroxide labels at higher temperature. As for all the other techniques requiring a freezing step, it
128 is assumed that the conformational ensemble of the sample is captured.
129

130   Since most of the available nitroxide-based spin labels can specifically react with the thiol group
131 of Cysteine, site-directed mutagenesis is often used to introduce Cys residues at specific locations in
132 the primary structure of the protein of interest.
133   *Hp*UreG has three naturally occurring Cys, located in different regions of the protein (Figure
134 1A): *i)* the conserved P-loop-motif, involved in GTP binding,[20] accommodates Cys7; *ii)* Helix 2,
135 involved in GTP-dependent conformational changes, contains Cys48[30]; *iii)* the fully conserved CPH
136 motif, involved in Ni(II) binding, includes Cys66.[20] These positions allow, in principle, to monitor the
137 mobility of three functionally important regions of the protein in solution. Consequently, six mutants
138 containing one or two Cys residues were designed and labeled with the MA-Proxyl nitroxide to
139 dissect the protein conformational landscape (Figure 1B): three double variants feature a unique
140 position available for labeling (C7^{prox}, corresponding to the Cys48Ser/Cys66Ala labeled mutant;
141 C48^{prox} corresponding to the Cys7Ala/Cys66Ala labeled mutant; C66^{prox}, corresponding to the
142 Cys7Ala/Cys48Ser labeled mutant), while three single variants possess two positions available for
143 labeling for distance measurements (C7^{prox}/C48^{prox}, corresponding to the Cys66Ala labeled mutant;
144 C7^{prox}/C66^{prox}, corresponding to the Cys48Ser labeled mutant; C48^{prox}/C66^{prox}, corresponding to the
145 Cys7Ala labeled mutant). Note that "WT^{prox}" corresponds to the wild-type protein (WT) labeled in

146 the three naturally occurring Cys residues. The labeling reactions were checked by Mass
147 Spectroscopy (see Figure S1 in the SI). Any possible perturbation of the global structure and of the
148 folding of *Hp*UreG mutations was excluded by controlling the global folding by circular dichroism
149 (CD, see Figure S2). Similarly, the catalytic activity of *Hp*UreG was monitored for the wild-type
150 protein labeled in the three Cys positions (WT^{prox}) (see Figure S1A), indicating no significant
151 differences between the unlabeled and labeled proteins (k_{cat} = 0.027
152 min^{-1} and k_{cat} = 0.023 min^{-1}, respectively).
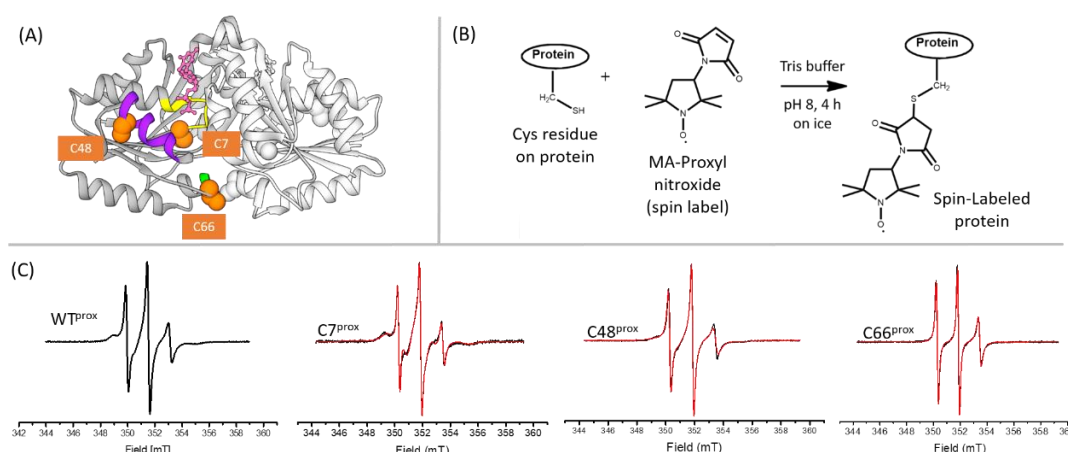
153

154

155 **Figure 1.** (A) *Hp*UreG structure in the presence of GDP (pink) from the *Hp*UreG$_2$F$_2$D$_2$ crystal (PDB
156 4HI0). The position of the three natural cysteine residues is highlighted in orange: Cys7 in the P-loop
157 (yellow), Cys48 in the Helix 2 (purple) and Cys66 in the CPH Nickel binding site (green). (B) Labeling
158 reaction scheme with MA-PROXYL nitroxide label. (C) Room temperature X-band EPR spectra of 50
159 μM of wild-type *Hp*UreG and its variants labeled with MA-PROXYL nitroxide in Tris buffer (black
160 trace) and superimposed simulated spectra (red traces).

161 *2.2. The thermodynamics of Ni(II) and GTP-driven dimerization of HpUreG was characterized*

162 Previous studies of Ni(II) binding to *Hp*UreG entailed the use of ITC, which showed that the
163 isolated protein interacts with two Ni(II) ions per monomer with an exothermic reaction and a
164 dissociation constant K_d = 10 μM.[20] Ni(II) binding was also monitored using the gradual increase of
165 absorption peak at 337 nm, assigned to ligand-to-metal-charge transfer.[29] Differently from the ITC
166 experiments, the latter approach did not detect any Ni(II) binding activity for the isolated protein,
167 whereas metal binding occurred when GTP was added to the protein solution, under which condition
168 *Hp*UreG was found to bind 0.5 equivalents of Ni(II) per protein monomer, with K_d = 0.33 μM, and to
169 undergo dimerization upon metal binding.[29]

170 Calorimetric titration of Ni(II) over a freshly purified *Hp*UreG sample, performed here for
171 comparison with all other ITC data on *Hp*UreG mutants and labeled forms described in the present
172 study, confirmed the results previously obtained by ITC, showing negative peaks following each
173 metal additions, indicative of an exothermic binding event (Figure 2A, left panel). The integrated heat
174 data generated a binding isotherm with a single inflection point, and a mild slope (Figure 2A, right
175 panel and Table 1). The fit of the obtained data, performed using the AFFINImeter software[46] and a
176 model involving a single set of sites, showed that two Ni(II) ions bind per *Hp*UreG monomer with
177 similar affinity (K_d = 72 μM), a favorable enthalpic contribution and a minor entropic impact (Table
178 1). Previously reported studies on *Hp*UreG mutants indicated that at least one Ni(II) binding site is
179 located on the CPH motif. [20, 29] These observations outline two possible scenarios: i) both Ni(II) ions
180 bind to identical sites located in the region of CPH, or ii) one Ni(II) ion binds to the CPH motif while
181 the second binds to different site; in the latter case, a possibility is represented by the Mg(II) binding

182 sites close to the GTP binding pocket, as previously suggested.[29] The difference in Ni(II) affinity thus
183 measured for *Hp*UreG (72 μM) with the previously reported value obtained by ITC (10 μM)[20] is likely
184 due to the experimental conditions: for the ITC titrations, the relatively weak metal-protein affinity
185 caused the value of the c-parameter, namely the product of the concentration of the protein in the cell
186 by the binding constant, to be close to its lowest acceptable limit,[20] rendering the calculated affinity
187 constants less accurate.
188

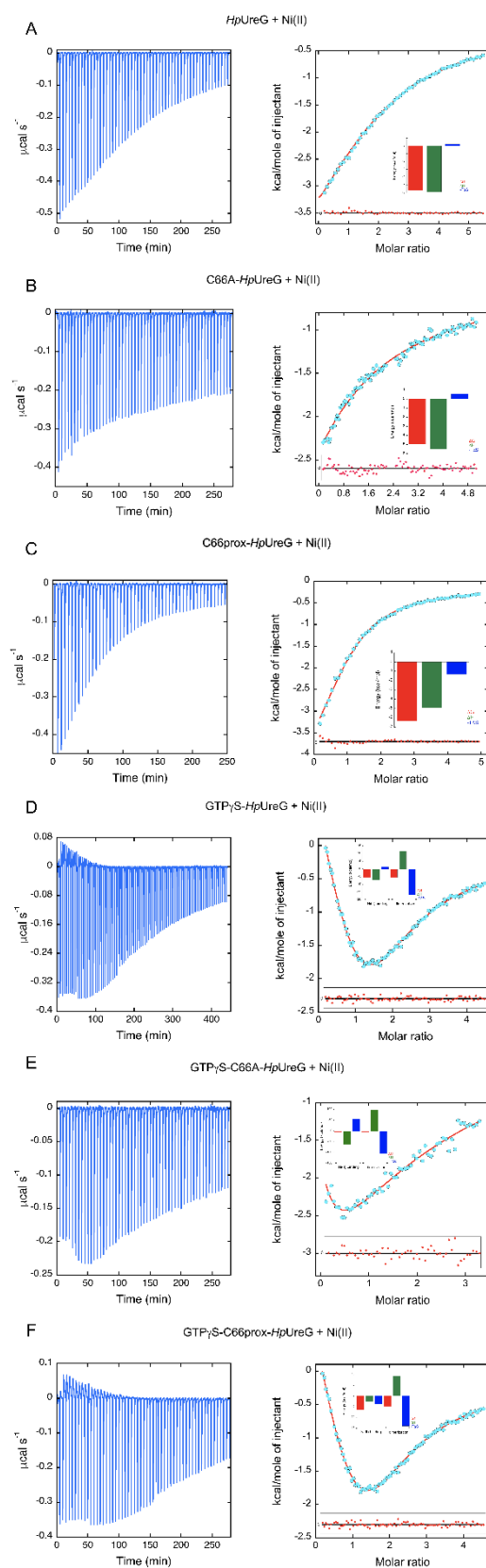**Figure 2.** ITC titrations of Ni(II) over *Hp*UreG and its variants in the presence and in the absence of GTPγS in the sample cell. The panels on the left report the heat flow response for the injections of the metal ion over the protein solutions. The panels on the right show the respective integrated heat data (blue circles) and their best fit obtained using a single set of binding sites (A, B, C) or a model involving

194   protein dimerization upon metal binding (D, E, F); the insets show the binding signatures (ΔG, ΔH, -
195   TΔS) associated to each curve; the bottom plots show the residuals of the fitting procedure.

196   Mutation of the Ni(II) binding residue Cys66 to Ala was previously reported to fully abolish
197   Ni(II) binding capability of the protein.[29] Here, the ITC titration instead revealed that the Cys66Ala-
198   *Hp*UreG mutant is still able to bind one Ni(II) ion per protein monomer, with an exothermic reaction
199   (Figure 2B, left panel) and one order of magnitude lower affinity (K_d = 236 μM), with substantially
200   invariant enthalpic and entropic contributions (Figure 2B, right panel and Table 1). This observation
201   suggests that the two Ni(II) binding sites per monomer, observed in wild-type *Hp*UreG, are distinct,
202   with one site, involving Cys66 in the CPH motif, that is abrogated by the Cys66-to-Ala mutation,
203   while the second is maintained. The decreased affinity for the latter site (K_d = 236 μM vs. 72 μM for
204   the mutated and WT protein, respectively) suggests the presence of cooperativity between the two
205   metal binding sites. The triply labeled WT[prox], while showing the same exothermic effect (Figure 2C,
206   left panel) and the same stoichiometry as the Cys66Ala mutant, features an higher affinity for Ni(II)
207   (K_d = 23 μM), a similar enthalpic value and positive entropic contribution (right panel of Figure 2C
208   and Table 1), as compared to the Cys66Ala mutant (K_d = 236 μM),   indicating that the Cys labeling
209   with the nitroxide moiety still abolishes one of the two Ni(II) binding sites observed for the unlabeled
210   WT protein, but, differently from the Cys66Ala mutation, maintains a similar affinity for the   second
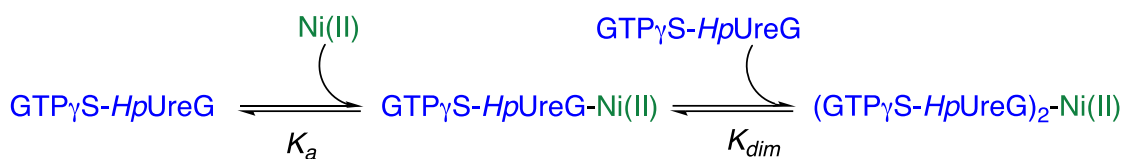211   Ni(II) binding event, supporting the idea of cooperativity between the two Ni-binding sites in the WT
212   protein.

Sample in the ITC cell	N	K_a (M^{-1})	K_d (μM)	ΔH (kcal mol^{-1})	ΔS (cal mol^{-1}K^{-1})
*Hp*UreG	2	1.38 ± 0.02 x 10^4	72 ± 1	-5.90 ± 0.06	-0.86
C66A-*Hp*UreG	1	4.23 ± 0.02 x 10^3	236 ± 1	-5.52 ± 0.01	-1.93
WT^{prox}-*Hp*UreG	1	4.33 ± 0.04 x 10^4	23.0 ± 0.3	-4.99 ± 0.02	4.47
*Hp*UreG-GTPγS	HpUreG-Ni	3.45 ± 0.02 x 10^4	30.0 ± 0.2	-7.14 ± 0.06	-4.99
	HpUreG$_2$-Ni	1.40 ± 0.04 x 10^4	71 ± 2	+11.2 ± 0.3	+56.77
C66A*Hp*UreG-GTPγS	C66AHpUreG-Ni	6.1 ± 0.8 x 10^3	160 ± 20	-61 ± 7	-187
	C66AHpUreG$_2$-Ni	4.5 ± 0.7 x 10^4	22 ± 3	+99 ± 9	+353
WT^{prox}-HpUreG-GTPγS	WT^{Prox}-HpUreG-Ni	4.20 ± 0.04 x 10^4	23.8 ± 0.2	-2.63 ± 0.03	+12.3
	WT^{Prox}-HpUreG$_2$-Ni	3.8 ± 0.3 x 10^3	260 ± 20	+9.1± 0.5	+46.8

214   **Table 1.** Thermodynamic parameters of Ni(II) titrations over *Hp*UreG and its variants, in the absence
215   and in the presence of GTPγS.

216   Ni(II)- and GTPγS -driven dimerization[29] was verified under the ITC experimental conditions
217   using size-exclusion chromatography coupled to multi-angle light scattering (SEC-MALS, Figure S3).
218   The obtained results confirmed that *Hp*UreG undergoes dimerization when both Ni(II) and GTPγS, a
219   non-hydrolyzable GTP analogue, are added to the protein solution, while it remains monomeric in
220   the presence of either Ni(II) or GTPγS alone.
221   The thermodynamics of Ni(II) and GTPγS-driven protein dimerization was therefore addressed
222   using ITC. Ni(II) ions were titrated over *Hp*UreG in the presence of GTPγS in the sample cell. Negative
223   peaks followed each injection of Ni(II) into the protein solution, indicating the occurrence of an
224   exothermic reaction (Figure 2D, left panel). The observation of a slower endothermic effect following
225   each injection, which terminates when one equivalent of metal is added to the protein solution,
226   suggested the existence of another process, in addition to metal binding, similarly to what had been
227   previously observed for the Ni(II)-sensor *Hp*NikR.[47] This type of ITC trace can be interpreted either
228   as a conformational modification or as a change in the oligomerization state of the protein. As
229   dimerization was demonstrated by light scattering experiments (Figure S3),[29] and the shape of the
230   binding isotherm clearly indicated two inflection points suggestive of two reactions occurring upon

231 metal titration, the data were analysed using a model involving two successive equilibria, with
232 protein dimerization following the binding of one Ni(II) per protein dimer (Scheme 1).
233

$$\text{GTP}\gamma\text{S-}HpUreG \underset{K_a}{\overset{\text{Ni(II)}}{\rightleftharpoons}} \text{GTP}\gamma\text{S-}HpUreG\text{-Ni(II)} \underset{K_{dim}}{\overset{\text{GTP}\gamma\text{S-}HpUreG}{\rightleftharpoons}} (\text{GTP}\gamma\text{S-}HpUreG)_2\text{-Ni(II)}$$

234

235 **Scheme 1**

236 Fitting of the binding isotherm (Figure 2D, right panel and Table 1) indicated that one Ni(II) ion
237 binds per protein monomer in the presence of GTPγS, with a dissociation constant two times smaller
238 than that reported for the apo-protein (K_d = 30 μM), while protein dimerization occurs with K_{dim} = 71
239 μM. In this case, Ni(II) binding occurs with thermodynamic parameters similar to the ones observed
240 for the apo-protein, with favorable enthalpy and a negative entropic contribution (Table 1). On the
241 other hand, dimerization is an entropy-driven endothermic process as expected (Table 1). The entire
242 two-step process is characterized by a global dissociation constant of K_d = 2 nM. This value should be
243 compared with that obtained by absorbance spectroscopy for Ni(II) binding to *Hp*UreG in the
244 presence of GTPγS (K_d = 0.33 μM)[29]. The difference between these two values could be attributed to
245 the different pH at which the measurements were carried out in the present (8.0) and in the previous
246 (7.2) work. The apparent decrease in affinity at lower pH is consistent with a proton dissociation
247 event occurring upon metal binding, which possibly involve a cysteine residue (Cys66 in this case),
248 as previously observed in the case of the nickel-dependent transcription factor *Hp*NikR.[47]
249 Ni(II) titration over the Cys66Ala mutant in the presence of GTPγS produced negative peaks
250 indicative of an exothermic binding of Ni(II), but no endothermic effect was visible (Figure 2E, left panel),
251 suggesting that a dimerization is either not occurring in this case or is occurring with much lower affinity
252 resulting in the absence of detectable endothermic heat. The binding isotherm (Figure 2E, right panel)
253 showed two inflection points, and the same model reported in Scheme 1 was used to treat the data.
254 According to the fit, the first event of Ni(II) binding occurs with one order of magnitude lower affinity
255 (K_d = 160 μM) as observed for the Cys66Ala mutant in the absence of GTPγS (Figure 2A), while the
256 second equilibrium shows a similar constant (K_d = 22 μM). In this case, the thermodynamic
257 parameters associated to the metal binding step and to the second process (Table 1) are unusually
258 high compared to all other similar data in this study, suggesting that additional phenomena other
259 than metal binding and dimerization are occurring in the case of this mutant. It is worth noticing that,
260 during sample manipulation, the Cys66Ala mutant was prone to precipitation, especially in the
261 presence of Ni(II), suggesting that at least part of the protein sample undergoes aggregation upon
262 Ni(II) titration, which might be the second process evidenced in the binding isotherm.
263 Ni(II) titration over the triply labeled WT[Prox] protein in the presence of GTPγS (Figure 2F, left
264 panel) produced a bipartite binding isotherm (Figure 2F, right panel), whose analysis, performed
265 according to Scheme 1, indicated that Ni(II) ion binding to the protein dimer occurs with an affinity
266 similar to the wild type protein (K_d = 23.8 μM), and favorable enthalpic and entropic contributions
267 (Table 1). On the other hand, the second process is less favorable for WT[Prox], occurring with a lower
268 equilibrium constant (K_d = 260 μM) as compared to the dimerization of the WT protein. If the second
269 process also involves dimerization for WT[Prox] (as suggested by the values of ΔH and ΔS, see Table 1)
270 this decreased value could be due to a steric effect of the nitroxide label.
271
272

273 *2.3. HpUreG shows distinct flexibility in different protein regions*

274 The EPR spectrum of WT *Hp*UreG labeled with MA-Proxyl nitroxide (WT[Prox], Figure 1C) arises
275 from the contribution of spin labels simultaneously grafted onto the three Cys residues. To separately

276 dissect the conformational flexibility of different regions of *Hp*UreG, the EPR spectrum of the
277 nitroxide-labeled *Hp*UreG variants that contain a single labeled cysteine (C7[prox], C48[prox], and C66[prox])
278 were performed in solution and at room temperature (Figure 1C). Qualitatively, when the nitroxide
279 mobility decreases, a broadening of the EPR spectral line shape is expected. For the single labeled
280 *Hp*UreG variants, the spectra show different mobility: the line shape becomes sharper going from
281 C7[prox] to C48[prox] and then to C66[prox], reflecting an increased mobility of the nitroxide moiety and,
282 consequently, of the protein structural motif to which the label is attached (Figure 1C). A quantitative
283 view of the nitroxide dynamics in terms of the rotational correlation time (τ_c) and of the magnetic
284 parameters (*g*-factor and hyperfine A-tensors) was obtained by simulating the EPR spectra with
285 SimLabel[48] (a MatLab graphical user interface using the Easyspin toolbox[49]) (see Table 2 and Section
286 2 in the SI). As very often found in SDSL-EPR studies,[27] the spectra of *Hp*UreG could be simulated by
287 two components, which represent populations of spin labels characterized by different dynamics.
288 These populations can be related either to rotameric states of the spin label or to structural sub-states
289 of the protein in conformational equilibrium. In the case of *Hp*UreG, the large difference in the
290 dynamics of the two components (see τ_c in Table 2), generally not observed for rotamers,[50] suggests
291 that they reflect distinct protein conformational states.[50-51] This conclusion is consistent with similar
292 phenomena reported for *Sp*UreG,[27] and is further supported by the observation that the *Hp*UreG EPR
293 spectrum of C66[prox] is modified by the addition of glycerol, a protective osmolyte: in this case, the
294 spectrum can be simulated by increasing the contribution of the slower component, which changes
295 from 44 to 70 % (Table 2 and Figure S4). Protective osmolytes are indeed known to modify the
296 conformational equilibria among different conformational states of the protein,[52] stabilizing the
297 protein structure toward a more folded conformation.[51]

298

Labeled site	Component	Apo-form		+ Ni(II)		+ Ni(II) and GTP	
		Weight %	τc (ns)	Weight %	τc (ns)	Weight %	τc (ns)
C66[prox]	Fast	56	0.6	34	0.6	28	0.7
	Slow	44	2.4	66	2.4	72	3.4
C66[prox] **+ gly 30%**	Fast	30	0.6	22	0.6	*19*	0.8
	Slow/Rigid*	70	2.4	78	2.4	81*	4.4*
C48[prox]	Fast	37	0.6	39	0.6	21	0.6
	Rigid	63	4.9	61	4.9	79	4.9
C7[prox]	Fast	20	0.3	15	0.3	14	0.3
	Rigid	80	6.1	85	6.1	86	6.1

299
300

301 **Table 2.** EPR spectra simulation parameters: rotational correlation times (τ_c in ns) and proportion (%)
302 of the simulated multi-components of the spectra of *Hp*UreG variants under various conditions.

303 The symbol (*) indicates the "rigid" component.

304

305 Note that, in the following paragraphs, we named "fast" all spectral components characterized
306 by τ_c values included between 0.3-0.7 ns, "slow" those characterized by τ_c values included between
307 0.7-4.0 ns and "rigid" components characterized by τ_c values included between 4.0-6.2 ns. The
308 sharpest EPR line shape is observed for the nitroxide grafted to Cys66. This spectrum is constituted
309 by two components having almost the same proportion, one with τ_c = 0.6 ns ("fast") and the other
310 with τ_c = 2.4 ns ("slow") (Table 2 and Figure 3). The fact that the "fast" component shows a mobility
311 close to that normally observed for a spin label attached to loops or intrinsically disordered protein

312 fragments [27, 41, 53] demonstrates that this region is highly flexible. This dynamic behaviour is similar to
313 that observed for the *Sp*UreG orthologue containing the nitroxide label grafted onto the
314 corresponding cysteine residue, which features two conformers with similar correlation times (τ_c
315 "fast" = 0.3 ns and τ_c "slow" = 3.6 ns) (see Figure S5).[27]
316   Similarly, two components with different degrees of flexibility and comparable relative
317 abundance are observed for C48^{prox}: one features a "fast" behavior (τ_c = 0.6 ns), while the other
318 ("rigid") is consistent with a less flexible dynamic (τ_c = 4.9 ns) (Table 2 and Figure 3). On the other
319 hand, a "rigid" component (τ_c = 6.1 ns) is dominant (80%) in the case of C7^{prox}, for which a less
320 abundant component (20 %) shows a "fast" behavior (τ_c = 0.3 ns) (Table 2 and Figure 3). The latter
321 case can be explained by considering that the nitroxide moiety resides in a well-structured region or
322 in a buried site. The high yield of labeling reached for this site (80-100%, Figure S1) suggests that
323 Cys7 is accessible, so the observed rigid behavior is indicative of the presence of a highly rigid protein
324 segment.
325   All these data experimentally confirm previously reported molecular dynamic simulations on
326 *Hp*UreG, which suggested substantial rigidity in the protein regions involved in catalysis, justifying
327 the residual catalytic activity of the isolated proteins, while evidenced the large dynamic flexibility
328 for the protein portions involved in protein−protein interactions, which contain the residues in the
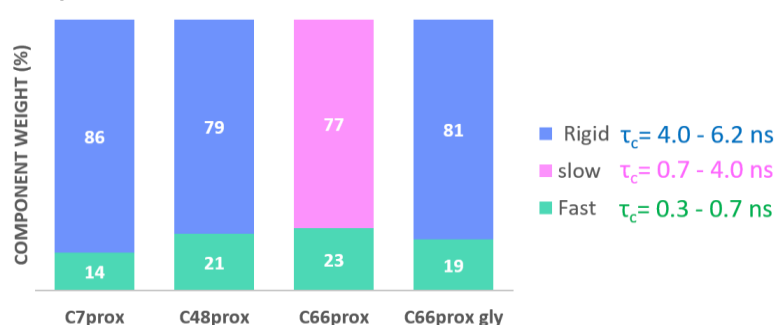329 conserved CPH motif.[54]
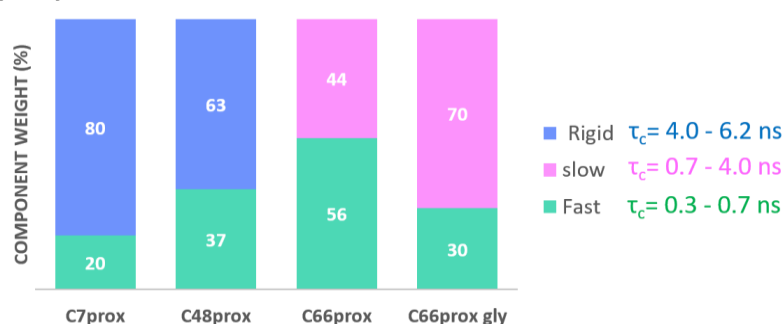
331 **Figure 3.** Conformational distribution of *Hp*UreG variants plotted in terms of the relative amount of
332 the conformations obtained from simulation of EPR spectra. The different conformational ensembles
333 are indicated using different colors and the relative correlation times are reported.

334   To further investigate the structural dynamics of *Hp*UreG in the apo-state, double electron-
335 electron resonance (DEER) experiments were applied. DEER experiments allow to measure the
336 dipolar coupling between spin pairs, yielding distance distribution between the coupled spins. Three
337 double-Cys variants were constructed and labeled (C7^{prox}/C48^{prox}, C7^{prox}/C66^{prox}, C48^{prox}/C66^{prox}) and
338 their CW EPR spectra are reported in Figure S7 in the SI. For all the DEER data shown in this section,
339 the error on distance distribution results was calculated with the validation tool of DeerAnalysis (see
340 Figure S8).[55] DEER data of the C7^{prox}/C48^{prox} variant (Figure 4A) showed well-resolved distance
341 distribution with 2 peaks centered at 2.4 and 3.5 nm, while the one obtained for C7^{proxyl}/C66^{proxyl}

342 (Figure 4B) and for C48[proxyl]/C66[proxyl] (Figure 4C) displayed broad distance distribution. These results
343 confirm the presence of considerable conformational heterogeneity in the protein sample, supporting
344 the highly flexible behavior of *Hp*UreG, as already observed by previous NMR studies[20] and by the
345 CW EPR data described above.
346 In all cases, the average distance distributions measured by DEER span a broader range than
347 those predicted by an MMM[56] analysis based on the *Hp*UreG crystal structure (PDB: 4HI10)[30] and a
348 library of rotamers for the MA-Proxyl spin label (Figure 4). This observation confirms that the
349 experimental conditions used in the crystallization experiments (solutes and salts acting as
350 precipitants) likely favored a more compact and rigid fold, as already shown for other biological
351 systems,[57] and that the protein structure observed in the crystal is different from the conformation
352 that the protein assumes in solution.
353
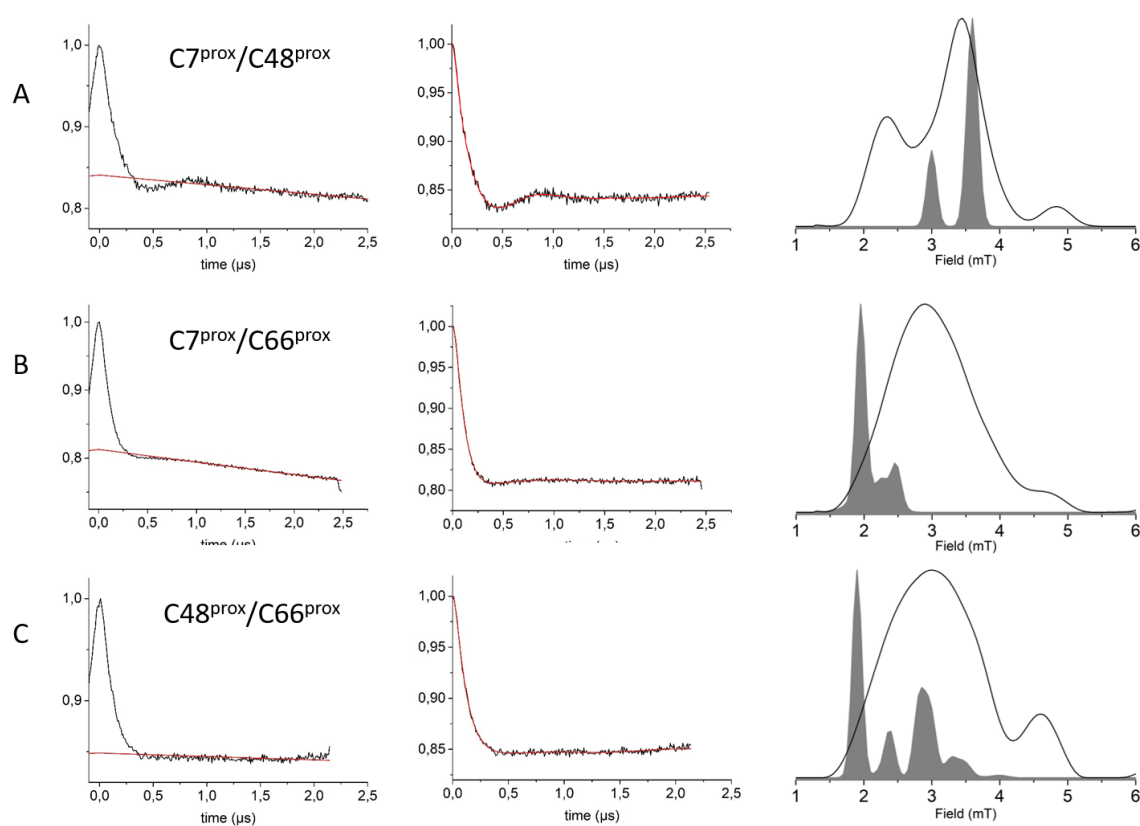

355 **Figure 4.** Inter-label distance distributions. <u>Left panel</u>: experimental Q-band DEER traces recorded at
356 60 K for (A) C7[prox]/C48[prox], (B) C7[prox]/C66[prox] and (C) C48[prox]/C66[prox]. Red lines indicate the baseline
357 used for background correction. <u>Central panel</u>: corrected DEER traces (black) with superimposed fits
358 derived from Tikhonov regularization (red). <u>Right panel</u>: Tikhonov derived distance distributions
359 obtained using DeerAnalysis (black)[55] superimposed with distance distributions calculated by MMM
360 software (gray curves).[56]

361

362 *2.4. Ni(II) ions and GTP binding produce changes in the structural dynamics of different protein regions*

363 Figure 5 shows the EPR spectra of the WT[prox] in the presence of either GTP or Ni(II), and in the
364 presence of both cofactors. No significant spectral changes were detected after the addition of either
365 GTP or Ni(II), while addition of both cofactors resulted in a clear change of the EPR line shape,

corresponding to an increase of the broader components of the spectrum. This indicates that both ligands are necessary to induce structural changes in *Hp*UreG.
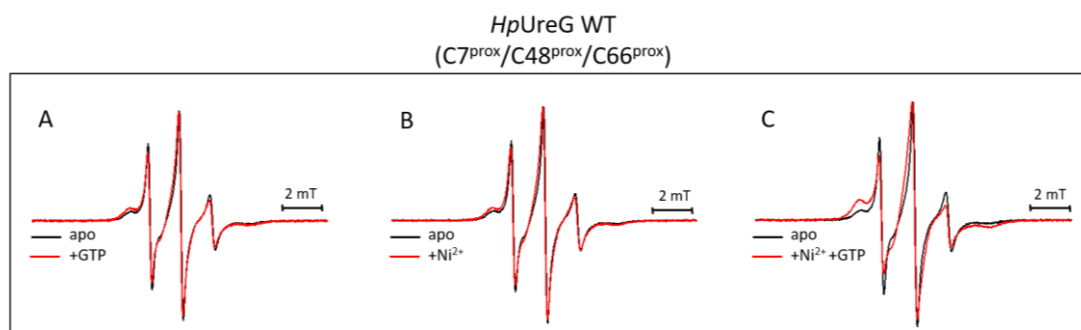

Figure 5. X-band CW EPR spectra of 50 μM *Hp*UreG labeled at the three naturally occurring Cys residues, recorded in solution and at room temperature. The apo-form spectra (black line) are compared to spectra recorded in presence of either 3 mM GTP and/or 2.5 mM Ni(II) (red line).

To investigate the source of this spectral modifications, and in particular to sort out which of the three nitroxide labels bound to the protein contributes to the Ni(II) and GTP-driven line broadening, the experiment was repeated using the single-Cys variants of *Hp*UreG.

Addition of Ni(II) did not produce significant changes of the EPR line shapes for C7[prox] (Figure 6A) and C48[prox] (Figure 6B), while for the C66[prox] spectrum induced a line broadening (Figure 6C) suggesting a reduction of the spin label mobility (Table 2 and Figure 3). Indeed, we observe a change in the weight of the two components (Table 2 and Figure 3), with the less flexible species becoming most abundant (from 44 to 66 %).

Differently, no significant spectral changes were detected on all protein variants after the addition of GTP or GDP alone (Figure S9 and S10). We also tested the effect of Mg(II) to protein samples containing GTP or GDP. The addition of Mg(II) in equimolar concentration with respect to GTP, did not affect the spectral shape of the protein (Figure S11 of SI).
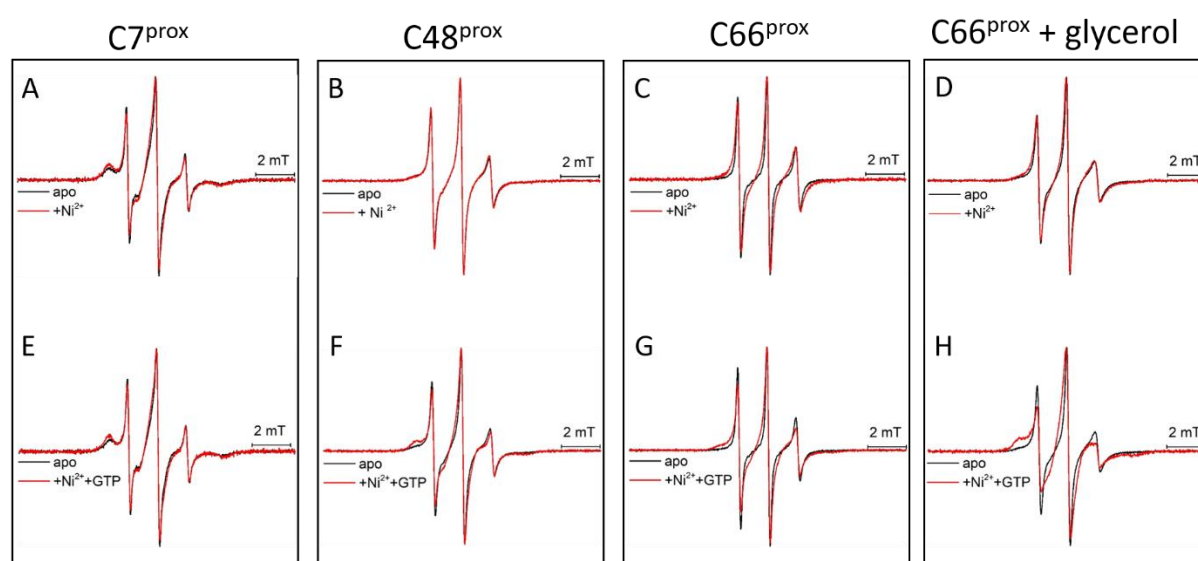

Figure 6. X-band CW EPR spectra of *Hp*UreG variants at room temperature, in the absence and in the presence of glycerol. In the upper panels the apo-form spectra are in black, those obtained in presence

389   of 2.5 mM of NiSO$_4$ are in red. The apo-form spectra (black line) are compared to spectra recorded in
390   presence of either 3 mM GTP and/or 2.5 mM Ni(II) (red line).

391   Concomitant addition of both Ni(II) and GTP did not significantly affect the spectrum of C7^{prox}
392   (Figure 6E), while it changed the line shape of C48^{prox} (Figure 6F), with a conformational shift toward
393   the "rigid" component, which increased from 63% to 79% (Table 2 and Figure 3). In the case of C66^{prox},
394   additional spectral changes were observed when GTP and Ni(II) bind to the protein; the τ_c of both
395   components increases, suggesting an induced structuration of this protein region (Table 2 and Section
396   2 of SI) or the dimerization of the protein upon both GTP and metal binding. These changes became
397   more pronounced if the experiments were performed in the presence of glycerol, with a drastic
398   change in the dynamics of the less flexible specie (Figure 6H, red trace), whose τ_c varies from 2.4 ns
399   to 4.4 ns (Table 2). These results were confirmed for the *Hp*UreG C48^{prox}/C66^{prox} variant, which
400   showed a similar behavior as found for C66^{prox} in glycerol (Figure S12).
401   The observed spectral changes indicate that Ni(II) and GTP induce structural and dynamics
402   modifications in the Ni(II)-binding region of the protein where C66 is located, and in the region
403   around Helix 2, containing C48. This suggests the occurrence of an allosteric communication between
404   the protein regions proximal to the Ni(II) and the GTP binding sites, whereas the region around the
405   Cys7 residue is not affected by the presence of either Ni or GTP, or both.
406   To further investigate the structural effect of ligand binding on *Hp*UreG fold, DEER experiments
407   would have been of great interest. However, the decrease in the T$_m$ (phase memory time) value
408   (Figure S13A) associated with the Field Sweep (FS) intensity loss (Figure S13B) in the presence of
409   Ni(II) prevented from obtaining properly exploitable DEER traces. Works are currently in progress
410   to improve the quality of DEER experiments.
411

412   **3.Conclusions**

413   In this work, the structural dynamics of *Hp*UreG was explored in the absence and in the presence
414   of its physiological cofactors, Ni(II) and GTP. In solution, *Hp*UreG fluctuates between different sub-
415   states, this plasticity likely being a key factor to allow the protein to perform protein-protein and
416   protein-metal ion interactions needed for Ni(II) ions delivery into the urease active site. ITC
417   determined the conditions and the thermodynamic parameters of Ni(II) and GTP-driven protein
418   dimerization, supported by light scattering data. SDSL-EPR demonstrated that the degree of
419   structural flexibility changes along the protein backbone, with the region involved in GTP binding
420   and the one involved in metal and protein interactions being more rigid and more flexible,
421   respectively. EPR also revealed that concomitant addition of both Ni(II) and GTP is necessary for a
422   structural transition in these two parts of the protein, located on opposite sides of the tertiary
423   structure, with a shift of the conformational equilibrium towards a more structured state. Differently,
424   addition of either the metal ions or the nucleotide produces only minor perturbations of the
425   conformational equilibrium, indicating that both ligands are necessary to exert a significant
426   conformational response. These observations suggest that binding of GTP in its pocket is propagated,
427   along the protein backbone, to the metal binding site where Ni(II) is bound, and *vice versa*. The
428   induced shift of the conformational ensemble of UreG likely regulates the protein function, possibly
429   allowing the protein to shuttle Ni(II) ions from UreE to the UreD$_2$-UreF$_2$ complex and, eventually, to
430   urease.
431   Overall, the present work represents an important contribution for the characterization of the
432   dynamics of UreG and its role in the network of the urease chaperone proteins. In the perspective to
433   extend this original approach, involving SDSL-EPR spectroscopy, to the study of urease network
434   directly inside bacterial cells, the results presented here provide important insights useful in the
435   research on molecules with anti-bacterial activities to overcome anti-microbial resistance (AMR).
436

437   **4. MATERIALS AND METHODS**

438 *4.1. Protein expression and purification*

439   The purification of *Hp*UreG and its mutants was performed using a protocol previously
440 reported.[58] We improved the yield of the protein expression growing the cells into auto-induction
441 medium containing glycerol (5 g/L), glucose (25 g/L) and lactose (100 g/L), instead than LB combined
442 with IPTG induction used in the previous work. The cells were growth 3 hours at 37 °C and 18 hours
443 at 28 °C. At the last step of purification, the proteins were in 20 mM TrisHCl pH 8 buffer, containing
444 NaCl 150 mM and TCEP 1 mM. Protein concentration was estimated using absorbance at 280 nm and
445 an extinction coefficient ε_{280}=10,032 $M^{-1}cm^{-1}$.

446 *4.2. Isothermal Titration Calorimetry*

447   Ni(II) binding titrations of wild-type and C66A mutant HpUreG were performed at 25 °C using
448 a high-sensitivity VP-ITC microcalorimeter (MicroCal). The protein and the metal ion salt ($NiSO_4$)
449 were diluted to 40-80 μM and 1.0 mM respectively into a solution of 20 mM TrisHCl pH 8, containing
450 150 mM NaCl and 1 mM TCEP, in the absence or in the presence of 150 μM of the non-hydrolyzable
451 GTP analogue, GTPYS. A reference cell was filled with deionized water. Before each experiment, the
452 baseline stability was verified. An interval of 5 minutes was applied between the injections to allow
453 the system to reach thermal equilibrium. Control experiments were conducted by titration of the
454 metal ion solution into the buffer alone under identical conditions, and the heat of dilution was
455 negligible. The solution containing the protein was loaded into a sample cell (1.4093 mL) and was
456 titrated with 55 x 5 μL injections with the Ni(II) solution. The raw data were processed and fitted
457 using Affinimeter software, with a nonlinear least-squares minimization algorithm to theoretical
458 titration curves with stoichiometric binding schemes. For Ni(II) titration over apo-HpUreG and C66A
459 mutant, restriction of the binding parameters had to be made by fixing the stoichiometry of 2 and 1
460 respectively, as the low affinity binding did not provide an optimal sigmoidicity of the curve with a
461 clear inflection point. Attempts to fit with stoichiometry of 1, 2, 3 and 4 were made, and the chosen
462 stoichiometry was the one that provided the best fit of the experimental data.

463 *4.3. HpUreG mutants design*

464   The cysteine mutations have been introduced into *Hp*UreG gene from Hp26695 strain urease
465 operon (NCBI code NC000915) cloned into the pET15b expression vector (Novagen) in a previous
466 work.[58]

467   In order to relate and compare this work with previous studies, Cys66, wen mutated, was
468 replaced by Alanine.[18, 29-30] We decided to perform a Cysteine-Serine mutation for position 48 to
469 preserve the surface charge of the protein, and a Cysteine-Alanine mutation in position 7 which is
470 more buried in the crystal structure.[22]

471   Mutants containing a single cysteine available for labeling were obtained by double mutation
472 (SI Table). They were named as following: *Hp*UreG-C7A-C48S: C66[proxyl]; *Hp*UreG-C7A-C66A:
473 C48[proxyl]; HpUreG-C66A-C48S: C7[proxyl].

474   Variants containing two labeling sites and thus needing only one cysteine mutated were
475 designed to perform distances measurements by DEER-EPR (SI Table) were named as following:
476 *Hp*UreG-C7A: C48[proxyl] /C66[proxyl]; *Hp*UreG-C66A: C7[proxyl]/C48[proxyl]; *Hp*UreG-C48S: C7[proxyl]/ C66[proxyl].

477 *4.4. GTP hydrolase activity assays*

478   *Hp*UreG GTP hydrolysing activity was measured by the SensoLyte® MG Phosphate Assay Kit
479 (AnaSpec), based on the colorimetric reaction involving malachite green reagent, molybdate and
480 orthophosphate.

481   Each sample was prepared mixing the reagents in order to obtain 20 μM of protein, 400 μM of
482 GTP and 2 mM of $MgSO_4$ in a final volume of 250 μL of buffer. The reaction mixture (RM) was
483 incubated for 2 hours at 37 °C. Every 30 minutes, 40 μL from the RM were incubated with 40 μL of
484 Malachite Green Mix for 10 minutes in a final volume of 300 μL of buffer. After incubation, the

485 absorbance at 600 nm was recorded. All the experiments were reproduced two times before estimate
486 the Kcat values**.**

4.5. Protein Labeling with nitroxide spin label

488 As *Hp*UreG variants are purified in presence of TCEP 1 mM, before labeling reaction, in order
489 to avoid the reduction of the nitroxide spin label, the reductant removal is necessary. In general, a gel
490 filtration using a PD-10 desalting column (GE Healthcare) is sufficient. The labeling procedure is
491 normally performed on 100 nmol of protein in a reductant-free buffer (Tris 20mM, pH=8, NaCl
492 150mM) in the presence of a 10-fold excess of nitroxide spin label, the maleimido-Proxyl (Sigma-
493 Aldrich). A 20-fold excess was used for double Cys variants. The mixture is then incubated at 4 °C,
494 in the dark for 4 hours under gentle stirring and continuous flow of argon. The excess of unbound
495 label is removed by a second gel filtration with a PD-10 desalting column. The labeled protein is
496 concentrated by using ultrafiltration (Vivaspin 5kDa, Sartorius). The concentration of the labeled
497 protein is evaluated by measuring the OD at 280 nm. The labeling yield of mono-labeled variants
498 analyzed was between 80% and 100%, 150-170% for double-labeled ones.

4.6. EPR spectroscopy

500 X-band room temperature (298 K) continuous wave EPR measurements were recorded on a
501 Elexsys500 Bruker spectrometer equipped with a Super High Q sensitivity resonator operating at X
502 band (9.9 GHz). The microwaves power was 10 mW, the magnetic field modulation amplitude was
503 0.1 mT, the field sweep was 15 mT, the receiver gain was 60dB. All the samples were analyzed in
504 quartz capillaries whose sensible volume was 40 µL.
505 The spin concentration was obtained by double integration of the EPR signal obtained under
506 non-saturating conditions and the labeling yield was evaluated comparing the spin concentration
507 with that one of a standard solution. For all variants, high labeling yields were obtained ranging from
508 80% to 100% for mono labeled samples and 150-170% for double-labeled samples.
509 X-band cw EPR spectra at room temperature were recorded at 50 µM of protein concentration
510 in Tris 20mM, pH=8, NaCl=150mM. When present, Ni(II) was 2.5mM (NiSO$_4$), GTP/GDP 3 mM
511 (Sigma-Aldrich).
512 The EPR spectra were simulated using SimLabel program,[48] a Matlab graphical user interface
513 using the Easyspin toolbox.[49]

4.7. DEER measurements

515 Inter-label distance distributions were obtained using the four-pulse DEER sequence.[59]
516 Experiments were performed on a Bruker ELEXSYS E580 spectrometer at Q-band using the standard
517 EN 5107D2 resonator. The system was equipped with an Oxford helium temperature regulation unit
518 and the data were acquired at 60K. This temperature has been optimized according to the relaxation
519 times measured at variable temperatures in the range of 20-100 K with 10 K steps. All the
520 measurements were performed on 20 µL of sample loaded into quartz capillaries. DEER samples
521 were flash frozen in liquid nitrogen. Distance distribution are extracted from DEER data through a
522 Tikhonov regularization after baseline correction, using DeerAnalysis2019 software
523 (http://www.epr.ethz.ch/software/index Jeschke G. 2011. DeerAnalysis. ETH Zürich).Distance
524 distribution measured were compared with the distance distributions predicted analyzing the crystal
525 of HpUreG (PDB 4HI0)[22] using the MMM software.[56]

Author contributions: Conceptualization, Barbara Zambelli and Elisabetta Mileo; Data curation, Guillaume
Gerbaud and Barbara Zambelli; Formal analysis, Emilien Etienne, Bruno Guigliarelli, Stefano Ciurli, Valérie
Belle and Barbara Zambelli; Funding acquisition, Stefano Ciurli and Elisabetta Mileo; Investigation, Annalisa
Pierro and Bruno Guigliarelli; Methodology, Annalisa Pierro; Project administration, Barbara Zambelli and
Elisabetta Mileo; Software, Emilien Etienne; Validation, Bruno Guigliarelli and Stefano Ciurli; Writing – original
draft, Stefano Ciurli, Valérie Belle, Barbara Zambelli and Elisabetta Mileo.

533

539

546

Supporting Information: Supporting figures and tables as well as detailed descriptions of all experimental procedures, comprising EPR spectra simulations, site-directed mutagenesis, measurement of UreG GTPase activity, Size exclusion chromatography and light scattering data, are provided with the manuscript.

<u>Section 1</u>: Supplementary figures (S1-S13), <u>Section 2</u>: CW spectra simulation with SimLabel program,

<u>Section 3</u>: Methods summary.

552

553

References.

1. Laxminarayan, R.; Duse, A.; Wattal, C.; Zaidi, A. K.; Wertheim, H. F.; Sumpradit, N.; Vlieghe, E.; Hara, G. L.; Gould, I. M.; Goossens, H.; Greko, C.; So, A. D.; Bigdeli, M.; Tomson, G.; Woodhouse, W.; Ombaka, E.; Peralta, A. Q.; Qamar, F. N.; Mir, F.; Kariuki, S.; Bhutta, Z. A.; Coates, A.; Bergstrom, R.; Wright, G. D.; Brown, E. D.; Cars, O., Antibiotic resistance-the need for global solutions. *The Lancet. Infectious diseases* **2013**, *13* (12), 1057-98.

2. Tornimbene, B.; Eremin, S.; Escher, M.; Griskeviciene, J.; Manglani, S.; Pessoa-Silva, C. L., WHO Global Antimicrobial Resistance Surveillance System early implementation 2016-17. *The Lancet. Infectious diseases* **2018**, *18* (3), 241-242.

3. https://www.who.int/medicines/publications/global-priority-list-antibiotic-resistant-bacteria/en/

4. Zambelli, B.; Musiani, F.; Benini, S.; Ciurli, S., Chemistry of Ni2+ in urease: sensing, trafficking, and catalysis. *Acc Chem Res* **2011**, *44* (7), 520-30.

5. Beenken, K. E.; Dunman, P. M.; McAleese, F.; Macapagal, D.; Murphy, E.; Projan, S. J.; Blevins, J. S.; Smeltzer, M. S., Global gene expression in Staphylococcus aureus biofilms. *J Bacteriol* **2004**, *186* (14), 4665-84.

6. Zhou, C.; Bhinderwala, F.; Lehman, M. K.; Thomas, V. C.; Chaudhari, S. S.; Yamada, K. J.; Foster, K. W.; Powers, R.; Kielian, T.; Fey, P. D., Urease is an essential component of the acid response network of Staphylococcus aureus and is required for a persistent murine kidney infection. *PLoS pathogens* **2019**, *15* (1), e1007538.

7. Jones, B. D.; Lockatell, C. V.; Johnson, D. E.; Warren, J. W.; Mobley, H. L., Construction of a urease-negative mutant of Proteus mirabilis: analysis of virulence in a mouse model of ascending urinary tract infection. *Infection and immunity* **1990**, *58* (4), 1120-3.

8. Gatermann, S.; Marre, R., Cloning and expression of Staphylococcus saprophyticus urease gene sequences in Staphylococcus carnosus and contribution of the enzyme to virulence. *Infection and immunity* **1989**, *57* (10), 2998-3002.

9. Ligon, J. V.; Kenny, G. E., Virulence of ureaplasmal urease for mice. *Infection and immunity* **1991**, *59* (3), 1170-1.

10. Zhou, F.; Yu, T.; Du, R.; Fan, G.; Liu, Y.; Liu, Z.; Xiang, J.; Wang, Y.; Song, B.; Gu, X.; Guan, L.; Wei, Y.; Li, H.; Wu, X.; Xu, J.; Tu, S.; Zhang, Y.; Chen, H.; Cao, B., Clinical course and risk factors for mortality of adult

583   inpatients with COVID-19 in Wuhan, China: a retrospective cohort study. *Lancet (London, England)* **2020,**
584   *395* (10229), 1054-1062.

585 11. Testerman, T. L.; Morris, J., Beyond the stomach: an updated view of Helicobacter pylori pathogenesis,
586   diagnosis, and treatment. *World journal of gastroenterology* **2014,** *20* (36), 12781-808.

587 12. Eaton, K. A.; Brooks, C. L.; Morgan, D. R.; Krakowka, S., Essential role of urease in pathogenesis of gastritis
588   induced by Helicobacter pylori in gnotobiotic piglets. *Infection and immunity* **1991,** *59* (7), 2470-5.

589 13. D'Elios, M. M.; Czinn, S. J., Immunity, inflammation, and vaccines for Helicobacter pylori. *Helicobacter* **2014,**
590   *19 Suppl 1*, 19-26.

591 14. Maroney, M. J.; Ciurli, S., Nonredox nickel enzymes. *Chem Rev* **2014,** *114* (8), 4206-28.

592 15. Mazzei, L.; Musiani, F.; Ciurli, S., CHAPTER 5 Urease. In *The Biological Chemistry of Nickel*, The Royal Society
593   of Chemistry: 2017; pp 60-97.

594 16. Ha, N.-C.; Oh, S.-T.; Sung, J. Y.; Cha, K. A.; Lee, M. H.; Oh, B.-H., Supramolecular assembly and acid
595   resistance of Helicobacter pylori urease. *Nature structural biology* **2001,** *8* (6), 505-509.

596 17. Tarsia, C.; Danielli, A.; Florini, F.; Cinelli, P.; Ciurli, S.; Zambelli, B., Targeting Helicobacter pylori urease
597   activity and maturation: In-cell high-throughput approach for drug discovery. *Biochimica et biophysica acta.*
598   *General subjects* **2018,** *1862* (10), 2245-2253.

599 18. Bellucci, M.; Zambelli, B.; Musiani, F.; Turano, P.; Ciurli, S., Helicobacter pylori UreE, a urease accessory
600   protein: specific Ni(2+)- and Zn(2+)-binding properties and interaction with its cognate UreG. *The*
601   *Biochemical journal* **2009,** *422* (1), 91-100.

602 19. Musiani, F.; Gioia, D.; Masetti, M.; Falchi, F.; Cavalli, A.; Recanatini, M.; Ciurli, S., Protein Tunnels: The
603   Case of Urease Accessory Proteins. *Journal of Chemical Theory and Computation* **2017,** *13* (5), 2322-2331.

604 20. Zambelli, B.; Turano, P.; Musiani, F.; Neyroz, P.; Ciurli, S., Zn2+-linked dimerization of UreG from
605   Helicobacter pylori, a chaperone involved in nickel trafficking and urease activation. *Proteins* **2009,** *74* (1),
606   222-39.

607 21. Fong, Y. H.; Wong, H. C.; Yuen, M. H.; Lau, P. H.; Chen, Y. W.; Wong, K.-B., Structure of UreG/UreF/UreH
608   Complex Reveals How Urease Accessory Proteins Facilitate Maturation of Helicobacter pylori Urease. *PLoS*
609   *biology* **2013,** *11* (10), e1001678.

610 22. Yuen, M. H.; Fong, Y. H.; Nim, Y. S.; Lau, P. H.; Wong, K.-B., Structural insights into how GTP-dependent
611   conformational changes in a metallochaperone UreG facilitate urease maturation. *Proceedings of the National*
612   *Academy of Sciences* **2017,** *114* (51), E10890-E10898.

613 23. Miraula, M.; Ciurli, S.; Zambelli, B., Intrinsic disorder and metal binding in UreG proteins from Archae
614   hyperthermophiles: GTPase enzymes involved in the activation of Ni(II) dependent urease. *J Biol Inorg*
615   *Chem* **2015,** *20* (4), 739-55.

616 24. Real-Guerra, R.; Staniscuaski, F.; Zambelli, B.; Musiani, F.; Ciurli, S.; Carlini, C. R., Biochemical and
617   structural studies on native and recombinant Glycine max UreG: a detailed characterization of a plant
618   urease accessory protein. *Plant molecular biology* **2012,** *78* (4-5), 461-75.

619 25. Zambelli, B.; Musiani, F.; Savini, M.; Tucker, P.; Ciurli, S., Biochemical studies on Mycobacterium
620   tuberculosis UreG and comparative modeling reveal structural and functional conservation among the
621   bacterial UreG family. *Biochemistry* **2007,** *46* (11), 3171-82.

622 26. Zambelli, B.; Stola, M.; Musiani, F.; De Vriendt, K.; Samyn, B.; Devreese, B.; Van Beeumen, J.; Turano, P.;
623   Dikiy, A.; Bryant, D. A.; Ciurli, S., UreG, a chaperone in the urease assembly process, is an intrinsically
624   unstructured GTPase that specifically binds Zn2+. *The Journal of biological chemistry* **2005,** *280* (6), 4684-95.

625 27. Palombo, M.; Bonucci, A.; Etienne, E.; Ciurli, S.; Uversky, V. N.; Guigliarelli, B.; Belle, V.; Mileo, E.;
626   Zambelli, B., The relationship between folding and activity in UreG, an intrinsically disordered enzyme.
627   *Scientific reports* **2017,** *7* (1), 5977.

628 28. D'Urzo, A.; Santambrogio, C.; Grandori, R.; Ciurli, S.; Zambelli, B., The conformational response to Zn(II)
629   and Ni(II) binding of Sporosarcina pasteurii UreG, an intrinsically disordered GTPase. *J Biol Inorg Chem*
630   **2014,** *19* (8), 1341-54.

631 29. Yang, X.; Li, H.; Lai, T.-P.; Sun, H., UreE-UreG Complex Facilitates Nickel Transfer and Preactivates GTPase
632   of UreG in Helicobacter pylori. *J. Biol. Chem.* **2015,** *290* (20), 12474-12485.

633 30. Fong, Y. H.; Wong, H. C.; Yuen, M. H.; Lau, P. H.; Chen, Y. W.; Wong, K. B., Structure of UreG/UreF/UreH
634   complex reveals how urease accessory proteins facilitate maturation of Helicobacter pylori urease. *PLoS*
635   *biology* **2013,** *11* (10), e1001678.

636 31. Merloni, A.; Dobrovolska, O.; Zambelli, B.; Agostini, F.; Bazzani, M.; Musiani, F.; Ciurli, S., Molecular
637 landscape of the interaction between the urease accessory proteins UreE and UreG. *Biochim Biophys Acta*
638 **2014,** *1844* (9), 1662-74.
639 32. Jeschke, G., The contribution of modern EPR to structural biology. *Emerging Topics in Life Sciences* **2018**.
640 33. Bordignon, E., EPR Spectroscopy of Nitroxide Spin Probes. In *eMagRes*, (eds R. K. Harris and R. L.
641 Wasylishen). ed.; 2017.
642 34. Roser, P.; Schmidt, M. J.; Drescher, M.; Summerer, D., Site-directed spin labeling of proteins for distance
643 measurements in vitro and in cells. *Organic & Biomolecular Chemistry* **2016,** *14* (24), 5468-5476.
644 35. Potapov, A.; Yagi, H.; Huber, T.; Jergic, S.; Dixon, N. E.; Otting, G.; Goldfarb, D., Nanometer-Scale Distance
645 Measurements in Proteins Using Gd3+ Spin Labeling. *Journal of the American Chemical Society* **2010,** *132* (26),
646 9040-9048.
647 36. Bonucci, A.; Ouari, O.; Guigliarelli, B.; Belle, V.; Mileo, E., In-Cell EPR: Progress towards Structural Studies
648 Inside Cells. *ChemBioChem* **2020,** *21* (4), 451-460.
649 37. Hubbell, W. L.; McHaourab, H. S.; Altenbach, C.; Lietzow, M. A., Watching proteins move using site-
650 directed spin labeling. *Structure (London, England : 1993)* **1996,** *4* (7), 779-83.
651 38. Hubbell, W. L.; Cafiso, D. S.; Altenbach, C., Identifying conformational changes with site-directed spin
652 labeling. *Nature structural biology* **2000,** *7* (9), 735-9.
653 39. Hubbell, W. L.; Lopez, C. J.; Altenbach, C.; Yang, Z., Technological advances in site-directed spin labeling
654 of proteins. *Curr Opin Struct Biol* **2013,** *23* (5), 725-33.
655 40. Le Breton, N.; Martinho, M.; Mileo, E.; Etienne, E.; Gerbaud, G.; Guigliarelli, B.; Belle, V., Exploring
656 intrinsically disordered proteins using site-directed spin labeling electron paramagnetic resonance
657 spectroscopy. *Frontiers in molecular biosciences* **2015,** *2*, 21.
658 41. Belle, V.; Rouger, S.; Costanzo, S.; Liquiere, E.; Strancar, J.; Guigliarelli, B.; Fournel, A.; Longhi, S., Mapping
659 alpha-helical induced folding within the intrinsically disordered C-terminal domain of the measles virus
660 nucleoprotein by site-directed spin-labeling EPR spectroscopy. *Proteins* **2008,** *73* (4), 973-88.
661 42. Martinho, M.; Fournier, E.; Le Breton, N.; Mileo, E.; Belle, V., Nitroxide spin labels: fabulous spy spins for
662 biostructural EPR applications. In *Electron Paramagnetic Resonance: Volume 26*, The Royal Society of
663 Chemistry: 2019; Vol. 26, pp 66-88.
664 43. Jeschke, G., DEER distance measurements on proteins. *Annual review of physical chemistry* **2012,** *63*, 419-46.
665 44. Schiemann, O.; Prisner, T. F., Long-range distance determinations in biomacromolecules by EPR
666 spectroscopy. *Quarterly reviews of biophysics* **2007,** *40* (1), 1-53.
667 45. Schmidt, T.; Walti, M. A.; Baber, J. L.; Hustedt, E. J.; Clore, G. M., Long Distance Measurements up to 160
668 A in the GroEL Tetradecamer Using Q-Band DEER EPR Spectroscopy. *Angew Chem Int Ed Engl* **2016,** *55*
669 (51), 15905-15909.
670 46. Pineiro, A.; Munoz, E.; Sabin, J.; Costas, M.; Bastos, M.; Velazquez-Campoy, A.; Garrido, P. F.; Dumas, P.;
671 Ennifar, E.; Garcia-Rio, L.; Rial, J.; Perez, D.; Fraga, P.; Rodriguez, A.; Cotelo, C., AFFINImeter: A software
672 to analyze molecular recognition processes from experimental data. *Anal Biochem* **2019,** *577*, 117-134.
673 47. Zambelli, B.; Bellucci, M.; Danielli, A.; Scarlato, V.; Ciurli, S., The Ni2+ binding properties of Helicobacter
674 pylori NikR. *Chemical communications (Cambridge, England)* **2007,** (35), 3649-51.
675 48. Etienne, E.; Le Breton, N.; Martinho, M.; Mileo, E.; Belle, V., SimLabel: a graphical user interface to simulate
676 continuous wave EPR spectra from site-directed spin labeling experiments. *Magnetic resonance in chemistry*
677 *: MRC* **2017,** *55* (8), 714-719.
678 49. Stoll, S.; Schweiger, A., EasySpin, a comprehensive software package for spectral simulation and analysis
679 in EPR. *Journal of magnetic resonance (San Diego, Calif. : 1997)* **2006,** *178* (1), 42-55.
680 50. López, C. J.; Fleissner, M. R.; Guo, Z.; Kusnetzow, A. K.; Hubbell, W. L., Osmolyte perturbation reveals
681 conformational equilibria in spin-labeled proteins. *Protein science : a publication of the Protein Society* **2009,** *18*
682 (8), 1637-52.
683 51. Flores Jiménez, R. H.; Do Cao, M. A.; Kim, M.; Cafiso, D. S., Osmolytes modulate conformational exchange
684 in solvent-exposed regions of membrane proteins. *Protein science : a publication of the Protein Society* **2010,** *19*
685 (2), 269-78.
686 52. Bolen, D. W., Effects of naturally occurring osmolytes on protein stability and solubility: issues important
687 in protein crystallization. *Methods (San Diego, Calif.)* **2004,** *34* (3), 312-22.
688 53. Mileo, E.; Lorenzi, M.; Erales, J.; Lignon, S.; Puppo, C.; Le Breton, N.; Etienne, E.; Marque, S. R.; Guigliarelli,
689 B.; Gontero, B.; Belle, V., Dynamics of the intrinsically disordered protein CP12 in its association with

690   GAPDH in the green alga Chlamydomonas reinhardtii: a fuzzy complex. *Molecular bioSystems* **2013**, *9* (11),
691   2869-76.

692 54. Musiani, F.; Ippoliti, E.; Micheletti, C.; Carloni, P.; Ciurli, S., Conformational fluctuations of UreG, an
693   intrinsically disordered enzyme. *Biochemistry* **2013,** *52* (17), 2949-54.

694 55. Jeschke, G.; Chechik, V.; Ionita, P.; Godt, A.; Zimmermann, H.; Banham, J. E.; Timmel, C. R.; Hilger, D.;
695   Jung, H., DeerAnalysis2006 –A Comprehensive Software Package for Analyzing Pulsed ELDOR Data. *Appl.*
696   *Magn. Reson., v.30, 473-498 (2007)* **2006,** *30*.

697 56. Jeschke, G., MMM: A toolbox for integrative structure modeling. *Protein science : a publication of the Protein*
698   *Society* **2018,** *27* (1), 76-85.

699 57. Sarver, J. L.; Zhang, M.; Liu, L.; Nyenhuis, D.; Cafiso, D. S., A Dynamic Protein-Protein Coupling between
700   the TonB-Dependent Transporter FhuA and TonB. *Biochemistry* **2018,** *57* (6), 1045-1053.

701 58. Barbara, Z.; Paola, T.; Francesco, M.; Paolo, N.; Stefano, C., Zn2+-linked dimerization of UreG from
702   Helicobacter pylori, a chaperone involved in nickel trafficking and urease activation. *Proteins: Structure,*
703   *Function, and Bioinformatics* **2009,** *74* (1), 222-239.

704 59. Pannier, M.; Veit, S.; Godt, A.; Jeschke, G.; Spiess, H. W., Dead-Time Free Measurement of Dipole–Dipole
705   Interactions between Electron Spins. *Journal of Magnetic Resonance* **2000,** *142* (2), 331-340.
706

707